IEEE Photonics Journal
An IEEE Photonics Society Publication

Open Access

Effects of Lateral Optical Confinement In GaN VCSELs With Double Dielectric DBRs

Volume 12, Number 2, April 2020

Rongbin Xu
Yang Mei
Huan Xu
Tianrui Yang
Leiying Ying
Zhiwei Zheng
Hao Long
Baoping Zhang
Jianping Liu

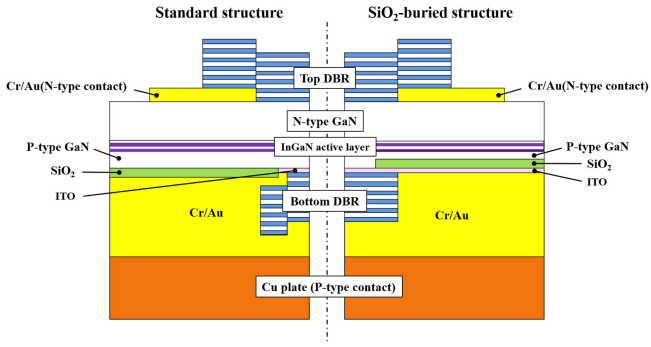

DOI: 10.1109/JPHOT.2020.2979564

Effects of Lateral Optical Confinement In GaN VCSELs With Double Dielectric DBRs

Rongbin Xu,[1] **Yang Mei**,[1] **Huan Xu**,[1] **Tianrui Yang**,[1] **Leiying Ying**,[1] **Zhiwei Zheng**,[1] **Hao Long**,[1] **Baoping Zhang**,[1] **and Jianping Liu** [2]

[1]Laboratory of Micro/Nano-Optoelectronics, Department of Electronic Engineering, School of Electronic Science and Engineering, Xiamen University, Xiamen 361005, China
[2]Suzhou Institute of Nano-tech and Nano-bionics, Chinese Academy of Sciences, Suzhou 215123, China

DOI:10.1109/JPHOT.2020.2979564

Manuscript received March 2, 2020; accepted March 5, 2020. Date of publication March 9, 2020; date of current version March 23, 2020. This work was supported in part by the Science Challenge Project under Grant TZ2016003 and in part by the National Key Research and Development Program of China under Grants 2016YFB0400803 and 2017YFE0131500. Corresponding author: Baoping Zhang (e-mail: bzhang@xmu.edu.cn).

Abstract: Two types of GaN vertical-cavity surface-emitting lasers (VCSELs), with and without lateral optical confinement (LOC) structure, were fabricated and their performances were compared. Compared with the VCSEL without LOC, the device with LOC showed a great improvement in threshold current, slope efficiency, output power and differential quantum efficiency, which was mainly due to the reduction of internal loss. Devices with LOC showed clear and multi-transversal mode structures. However, thermal dissipation became worse. The effects of such a design on thermal resistance and transverse modes were discussed.

Index Terms: Semiconductor lasers, vertical cavity surface emitting lasers, lateral optical confinement.

1. Introduction

GaN-based vertical-cavity surface-emitting lasers (VCSELs) are being heavily investigated due to their potential applications in visible light communication, microprojector and display [1], [2]. In recent years, several academic and industrial research groups have demonstrated electrically pumped GaN-based VCSELs [3]–[11]. However, the performance of GaN-based VCSELs is still not good enough and challenges are necessary in such as achieving high-reflectivity mirrors, efficient lateral current spreading and lateral optical confinement (LOC) [12]. Further improvements in GaN-based VCSELs are required toward applications.

The LOC plays an important role in improving the efficiency, as suggested by the development history of infrared VCSELs [13], [14]. The devices do not contain optical guiding structures will suffer from higher diffraction loss because of the divergent distribution of the optical field, which will cause low energy conversion efficiency [15], [16]. Basically, an index-step core-cladding structure like an optical fiber is required for the optical guiding. In commercialized GaAs-based VCSELs, selective lateral oxidation of a semiconductor layer with high aluminum content like $Al_{0.98}Ga_{0.02}As$ or even AlAs is employed for realization of optical guiding and current confinement as well. However, in GaN-based VCSELs, selective lateral oxidation is impossible. Therefore, the formation

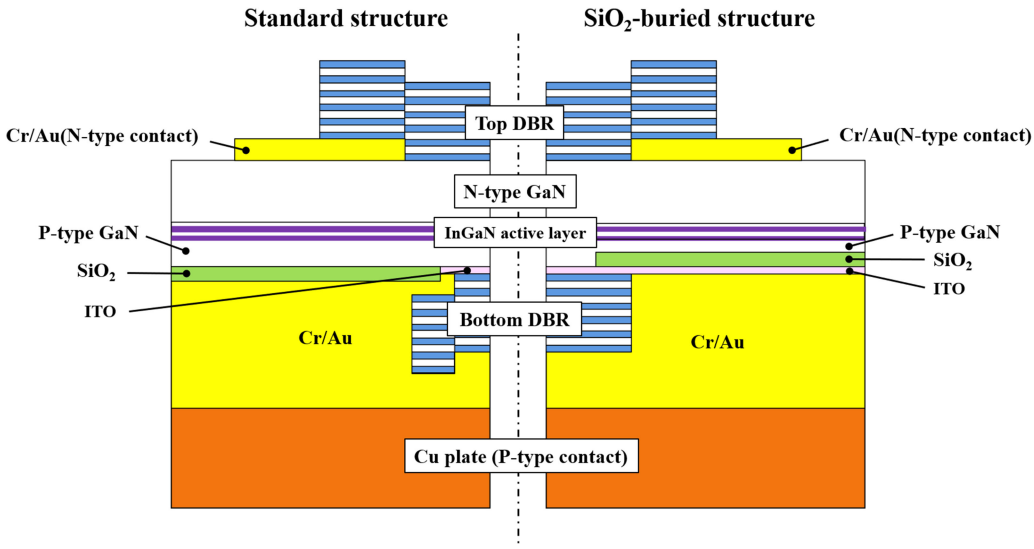

Fig. 1. Schematic of the VCSEL with the standard structure (left half) and the SiO_2-buried structure (right half).

of the LOC structure in GaN-based VCSELs is rather complex since this structure can result in anti-guiding [16]. In recent years, several approaches have been used to obtain the GaN-based VCSELs with LOC structure. Leonard *et al.* [17]. used ion implantation to enabling a planar ITO design of intra-cavity structure. The refractive index decreases due to implantation, which is favorable for providing optical confinement in the aperture. After that, they reported an air-gap formed by the photoelectrochemically (PEC) etching to selectively remove the active region outside the aperture area [18]. This approach also achieved a large index contrast between core and the lateral cladding of the device. However, these approaches may damage the wafer and has a high cost. Kuramoto *et al.* [19]. introduced a SiO_2-buried structure in GaN-based VCSEL with hybrid epitaxial/dielectric distributed Bragg reflector (DBR). The reported devices showed a high output power of 6 mW. The author attributed this as a result of reduction of the internal loss by LOC structure and adjustment of the front mirror reflectivity. Compared with GaN VCSELs with epitaxial AlGaN/GaN or AlInN/GaN DBR, the precise control of cavity length using a thinning process is difficult for devices with two dielectric DBRs. In 2018, Hamaguchi *et al.* [20] used a curved mirror formed monolithically on a GaN wafer to achieve LOC. They conclude that this approach allows aperture miniaturization to the diffraction limit, and a relatively long cavity can be used due to the reduction of diffraction loss.

In this work, a thick SiO_2-buried structure was used to form the LOC in GaN-based VCSELs with double dielectric DBRs. We present the testing results and compare the results with the standard structure VCSELs. The effects of such a design were analyzed from the point of internal loss and thermal property. In addition, the transverse mode characteristics were discussed for the devices with different aperture sizes.

2. Materials and Methods

The adopted epitaxial structure was grown on a c-plane sapphire substrate by using metal-organic chemical-vapor deposition. The active region consisted of two periods of $In_{0.18}Ga_{0.82}N$ (2.5 nm)/GaN (6 nm) quantum wells (QWs). A 20 nm $Al_{0.2}Ga_{0.8}N$ layer was used as electron blocking layer. As illustrated in the right half of Fig. 1, the VCSEL demonstrated here employed a dual dielectric DBR design and SiO_2 aperture/ITO electrode structure. The SiO_2-buried structure was fabricated by etching a patterned groove of the p-GaN layer to a depth of 200 nm using

TABLE 1
Differences of Two Structure VCSELs

Structure	Standard structure	SiO_2-buried structure
LOC	No	Yes
Effective cavity length (nm)	3986	2886
Pairs of top/bottom DBRs	11/13.5	10/12.5
Reflectivity of top/bottom DBRs	99.88%/99.95%	99.24% /99.89%

ICP etching, and a 200 nm SiO_2 film was deposited by magnetron sputtering. Devices with 8 μm and 15 μm current confinement apertures were fabricated. For comparison, a standard structure VCSEL with dual dielectric DBRs is also shown in the left half of Fig. 1, where the SiO_2 film with the same thickness was deposited on the p-type GaN directly. SiO_2 and TiO_2 were used as low and high refractive index materials of mirrors. The refractive indexes of SiO_2 and TiO_2 are 2.45 and 1.46, respectively. The pairs of top and bottom DBRs are shown in Table 1. Cr/Au was used for both p- and n-type electrodes of both structures.

According to the effective index model [21], the relative refractive index difference $\Delta n/n$ can be estimated from the local resonance wavelength shift between the center and peripheral regions of the VCSEL mesa, as described by the following equation

$$\frac{\lambda_c - \lambda_p}{\lambda_c} = \frac{\Delta\lambda}{\lambda_c} = \frac{\Delta n}{n} \tag{1}$$

where λ_c and λ_p are the resonance wavelengths of the center and peripheral areas, respectively. When $\lambda_c - \lambda_p$ is positive, the optical guiding is obtained. λ_c and λ_p can be obtained from the calculated reflectivity spectrum of an entire VCSEL cavity by transfer matrix simulation [22]. By the calculation, $\Delta n/n$ of SiO_2-buried structure VCSEL is 0.027. On the contrary, $\Delta n/n$ is -0.054 for the standard structure VCSEL, showing the anti-guiding. The differences of fabricated devices are summarized in the Table 1. The reflectivity of top and bottom DBRs was measured by spectrophotometer. Effective cavity length L_{eff} was estimated from the measured longitudinal mode spacing $\Delta\lambda_L$ [22]

$$\Delta\lambda_L = \frac{\lambda_c^2}{2nL_{eff}}\left(1 - \frac{\lambda_c}{n}\frac{dn}{d\lambda}\right)^{-1} \tag{2}$$

where n is the refractive index, $dn/d\lambda = -0.001$. Different effective cavity length of the two structure devices comes from the different thickness of n-type GaN layer and the DBR penetration depth.

3. Results and Discussion

The VCSELs with a 15 μm aperture diameter were tested under continuous-wave (CW) operation at room temperature (RT). Figs. 2 and 3 show the emission spectra of devices with different structures under different current levels, together with the corresponding current–light output (I-L) curves and polarization characteristics. Multi-longitudinal mode lasing was observed for both structure VCSELs and the emission wavelength shows a little redshift due to the heating effect. To estimate the Q value of the resonant cavity, the linewidths of emission modes were measured below threshold current with a higher resolution of 0.015 nm, as shown in the inset of Figs. 2(a) and 3(a). We also applied linear fits to the I-L data and the threshold currents were extracted. Polarization measurements show that the degree of polarization of standard and SiO_2-buried structure devices

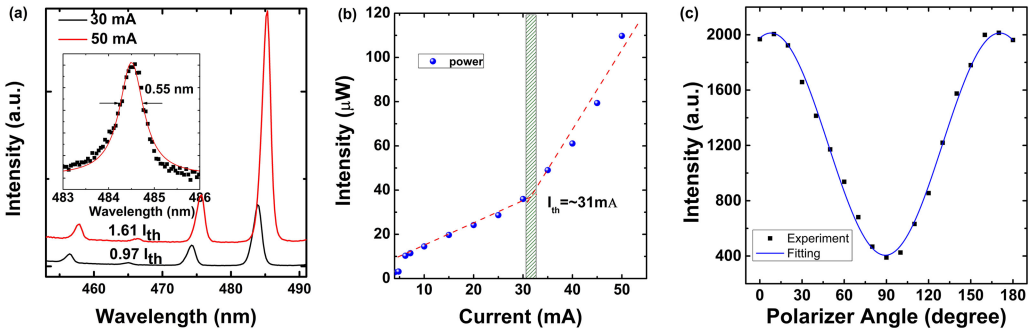

Fig. 2. (a) The emission spectra of the standard structure VCSEL at injection current of 0.97 I_{th} and 1.61 I_{th}, respectively. The inset exhibits the linewidth of the emission mode measured with a higher resolution at 20 mA. (b) The light output as a function of injection current at 300 K and CW operation. (c) Polarization characteristics of the laser emission.

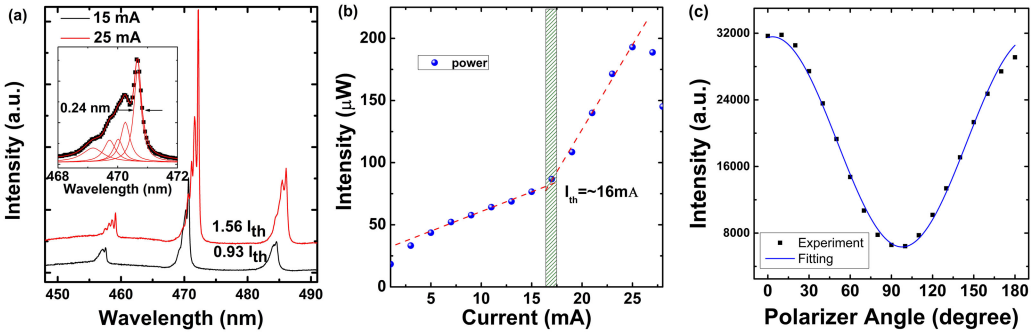

Fig. 3. (a) The emission spectra of the SiO_2-buried structure VCSEL at injection current of 0.93 I_{th} and 1.56 I_{th}, respectively. The inset exhibits the linewidth of the emission mode measured with a higher resolution at 15 mA. (b) The light output as a function of injection current at 300 K and CW operation. (c) Polarization characteristics of the laser emission.

TABLE 2
Measurement Results of Two Structure VCSELs at RT

Structure	Standard structure	SiO_2-buried structure
Threshold current (mA)	31	16
Maximum output power (μW)	110	200
Slope efficiency (W/A)	0.0036	0.013
Thermal roll-over current (mA)	50	26

are 71% and 69% under CW operation of 1.1I_{th}, respectively. In addition, multi-transverse modes can be observed associated with each single longitudinal mode for the SiO_2-buried structure only. More details about transverse mode characteristics will be discussed in the later part of the article.

The measurement results of the VCSELs with and without LOC are summarized in Table 2. As shown in Table 2, the SiO_2-buried structure VCSELs have lower threshold current and higher maximum output power than the standard VCSELs. The improvements of the VCSEL with LOC could be attributed to the reduction of the intra-cavity losses. At the same time, the reduction of

TABLE 3
VCSEL Parameters Obtained From Calculation

Structure	Standard structure	SiO_2-buried structure
Total loss (cm^{-1})	362	169
Mirror losses (Top/Bottom) (cm^{-1})	1.5/0.63	13.2/1.9
Internal loss (cm^{-1})	359.87	153.9
Differential quantum efficiency (%)	0.14	0.49
Injection efficiency (%)	33.8	6.3

the top mirror reflectivity from 99.88% to 99.24% will also benefit to achieve a high slope efficiency, and finally a high output power. However, the SiO_2-buried structure VCSELs have a low thermal roll-over current, which suggests that the thermal dissipation is worse.

The total loss α_{total} of the VCSEL is roughly divided into mirror loss α_m and internal loss α_i. To gain insight into the advantages introduced by using the LOC structure, we calculated the losses introduced by the DBR and the resonant cavity. The loss of top/ bottom DBR $\alpha_m^{T/B}$ can be expressed in terms of effective cavity length L_{eff} and the reflectivity $R_{T/B}$ as [23]

$$\alpha_m^{T/B} = \frac{1}{2L_{eff}} \ln\left(\frac{1}{R_{T/B}}\right) \tag{3}$$

The calculated L_{eff} and measured $R_{T/B}$ are shown in Table 1. The total mirror loss consists of top and bottom DBR losses. The α_i value can be estimated from the measured quality factor Q of the resonant cavity [24]

$$\alpha_{total} = \alpha_i + \alpha_m = \frac{2\pi n}{\lambda_c Q} \tag{4}$$

As shown in the inset of Figs. 2(a) and 3(a), the linewidth of the emission modes was measured to be 0.24 nm and 0.55 nm for the device with and without LOC, respectively. The corresponding Q values are 1963 and 880.

We also analyzed the injection efficiency η_i of the devices, which indicates the fraction of injected carriers converted into photons according to the formula [23]

$$\eta_d = \eta_i \times \frac{\alpha_m^T}{\alpha_i + \alpha_m^T + \alpha_m^B} \tag{5}$$

The differential quantum efficiency η_d in the equation can be extracted from the L-I curves via its relation to the slope efficiency dP/dI

$$\eta_d = \frac{q}{h \times \upsilon} \times \frac{dP}{dI} \tag{6}$$

where q is the electron charge, h is Planck's constant, and υ is the laser frequency. The calculated results are summarized in Table 3. The internal loss in a standard structure is more than two times higher compared with the SiO_2-buried structure. It has been reported that the impact of transverse radiation loss was an extremely high value that occupies more than 2/3 of the whole internal loss in the standard VCSELs [25], since the absorption loss do not vary much between the different cavity structures. The internal loss of the VCSEL incorporating a LOC structure was significantly reduced due to the decrease of transverse radiation loss. On the other hand, the mirror loss only occupies a small part of the total loss for both structures. An appropriate reduction of the DBR

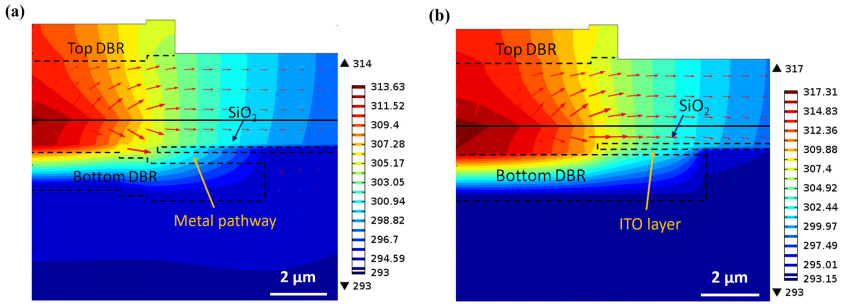

Fig. 4. COMSOL thermal simulation of a 10 μm aperture diameter VCSEL with (a) standard structure and (b) SiO_2-buried structure. The color scheme represents the increase in temperature and the overlain arrows represent the thermal flux.

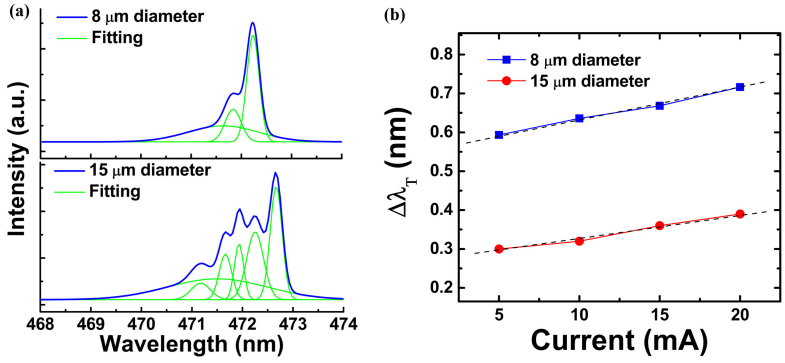

Fig. 5. (a) Emission spectra of devices with 8 μm and 15 μm aperture size (b) Wavelength separation between zeroth and first order modes as a function of increasing current.

reflectivity is feasible for VCSELs with LOC structure to achieve a high output power. However, the injection efficiency of the SiO_2-buried structure was much lower, 6.3%. The η_i value was decreased possibly due to the structure incorporated LOC have smaller spot sizes where peripheral current might be wasted. Moreover, due to the relatively short cavity length, resulting in the relatively poor heat dissipation. Free-carrier absorption is higher at higher temperature.

The thermal characteristics of GaN-based VCSEL will be affected by the device structure such as cavity length, mesa size, as well as bottom DBR size [25]. Fig. 4 presents the thermal performance of the standard structure and SiO_2-buried structure VCSELs. The color scheme shows the increase in temperature after reaching the steady-state. The method of calculation and the thermal conductivities of the materials were same as our previous work [26]. The temperature of bottom surface of the substrate was set to be room temperature (293 K) as a boundary condition during the simulation. The model predicted an active region temperature of 313.63 °C for the standard structure and 317.31 °C for the SiO_2-buried structure. The thermal resistance R_{th} could be obtained by $R_{th} = \Delta T/U_{th} \cdot I_{th}$, where U_{th} and I_{th} are threshold voltage and threshold current, respectively. Here, U_{th} was set to be 4.5 V and I_{th} was set to be 8 mA. The thermal resistance R_{th} was calculated to be 573 K/W and 675 K/W for the two structures. The R_{th} value of SiO_2-buried structure is bigger than that of standard structure. For standard structure, thermal energy could spread out over the cavity in lateral direction by intra-cavity metal pathway, but for SiO_2-buried structure without metal pathway, heat transfer in lateral direction is impeded due to the low thermal conductivity of ITO layer. The increased thermal resistance also affects the heat dissipation of the device, which jointly results in the reduction of the peak injection current and injection efficiency.

Multi-transverse modes were observed in the VCSEL with LOC. In Fig. 5(a), the spectra of devices with 8 μm and 15 μm aperture size are fitted by multi-Lorentzian peaks. Less small peaks are observed in 8 μm aperture device since higher-order modes have more of their intensity extend

outside the small optical confinement aperture. Higher order modes are more likely to appear in the devices with large aperture size. In addition, the spacing between transverse modes as a function of current was also discussed, as shown in Fig. 5(b). For an almost planar resonator, such as VCSEL with DBRs, the mode spacing is given by [27]

$$\Delta\upsilon = \frac{c\lambda_c}{2\pi^2 n^2 \omega_0^2} \propto \frac{cL_{eff}}{\pi^2 n \omega_0^2} \tag{7}$$

where c is the speed of light, n is refractive index and ω_0 is the minimum spot size of the fundamental mode. Substitution of the definition of the wavelength, $\lambda_c = 2nL_{eff}/m$, gives an expression in terms of refractive index and effective cavity length [5]. Here, m is a positive integer. Note that the mode spacing of the devices increases with increasing currents. From (7), it is seen that the mode spacing is affected by the effective cavity length, refractive index and mode spot size. The temperature inside the cavity will increase with increasing the injection current. Due to the small thermal expansion coefficient of GaN film, however, the effective cavity length is almost unchanged. n is known to increase at higher currents as demonstrated by the redshift of the emission modes. Therefore, an increase in the mode spacing with injection current can only be explained by considering that the mode spot size is decreasing faster than the increase of n. The decrease of the mode size, called thermal lensing, is originated from the inhomogeneous index profile caused by increasing current and, probably, composition fluctuation as well [27]. In addition, it is found that the rate of change with current of the mode separation ($\Delta\lambda_T/\Delta I$) is higher for the devices with small aperture size. For example, $\Delta\lambda_T/\Delta I$ for 8 μm aperture device is $\sim$0.008 nm/mA, while for 15 μm diameter device, it is $\sim$0.005 nm/mA. The thermal lens effect of 8 μm devices is more pronounced since the current density of the small VCSEL is relatively high, causing more heating. However, it had been reported that the thermal lens effect will strongly affect the efficiency of the device [28]. Therefore, it is to be expected that a small current aperture device with a long cavity length (good heat dissipation) will be helpful to achieve high performance VCSEL with single transverse mode.

4. Conclusion

In summary, we comparatively studied GaN-based VCSELs with and without LOC structure. The experiment results show that the device with LOC structure has lower threshold current and higher output power, owing to the reduction of the internal loss. Although higher thermal resistance is obtained compared with the standard structure, improvement should be possible by increasing the cavity length. Finally, the observed transverse mode characteristics were affected by the aperture size and the heat dissipation of the device. This work provides a better understanding of the optical and thermal property of GaN-based VCSELs with such a typical structure and is useful in optimizing the structure design and improving the device performance.

References

[1] D. F. Feezell, "Status and future of GaN-based vertical-cavity surface-emitting lasers," in *Proc. Gallium Nitride Mater. Devices X*, San Francisco, CA, USA, 2015, Art. no. 93631G-1.
[2] H. C. Yu *et al.*, "Progress and prospects of GaN-based VCSEL from near UV to green emission," *Prog. Quantum Electron.*, vol. 57, pp. 1–19, Feb. 2018.
[3] T. C. Lu, C. C. Kao, H. C. Kuo, G. S. Huang, and S. C. Wang, "CW lasing of current injection blue GaN-based vertical cavity surface emitting laser," *Appl. Phys. Lett.*, vol. 92, no. 14, Apr. 2008, Art. no. 141102.
[4] D. Kasahara *et al.*, "Demonstration of blue and green GaN-based vertical-cavity surface-emitting lasers by current injection at room temperature," *Appl. Phys. Express*, vol. 4, no. 7, Jul. 2011, Art. no. 072103.
[5] T. Onishi, O. Imafuji, K. Nagamatsu, M. Kawaguchi, K. Yamanaka, and S. Takigawa, "Continuous wave operation of GaN vertical cavity surface emitting lasers at room temperature," *IEEE J. Quantum Electron.*, vol. 48, no. 9, pp. 1107–1112, Jun. 2012.
[6] K. Ikeyama *et al.*, "Room-temperature continuous-wave operation of GaN-based vertical-cavity surface-emitting lasers with n-type conducting AlInN/GaN distributed Bragg reflectors," *Appl. Phys. Lett.*, vol. 9, no. 10, Oct. 2016, Art. no. 102101.

[7] P. S. Yeh *et al.*, "GaN-based vertical-cavity surface emitting lasers with sub-milliamp threshold and small divergence angle," *Appl. Phys. Lett.*, vol. 109, no. 24, Dec. 2016, Art. no. 241103.
[8] Y. Mei *et al.*, "Quantum dot vertical-cavity surface-emitting lasers covering the 'green gap'," *Light, Sci. Appl.*, vol. 6, Jan. 2016, Art. no. e16199.
[9] C. A. Forman *et al.*, "Continuous-wave operation of m-plane GaN-based vertical-cavity surface-emitting lasers with a tunnel junction intracavity contact," *Appl. Phys. Lett.*, vol. 112, no.11, Mar. 2018, Art. no. 111106.
[10] M. Kuramoto *et al.*, "High-output-power and high-temperature operation of blue GaN-based vertical-cavity surface-emitting laser," *Appl. Phys. Express*, vol. 11, no. 11, Nov. 2018, Art. no. 112101.
[11] S. M. Mishkat-Ul-Masabih, A. A. Aragon, M. Monavarian, T. S. Luk, and D. F Feezell, "Electrically injected nonpolar GaN-based VCSELs with lattice-matched nanoporous distributed bragg reflector mirrors," *Appl. Phys. Express*, vol. 12, no. 3, Mar. 2019, Art. no. 036504.
[12] Å. Haglund *et al.*, "Progress and challenges in electrically pumped GaN-based VCSELs," in *Proc. Semicond. Lasers Laser Dyn. VII*, Brussels, Belgium, 2016, Art. no. 98920Y-1.
[13] B. Weigl *et al.*, "High-performance oxide-confined GaAs VCSELs," *IEEE J. Sel. Topics Quantum*, vol. 3, no. 2, pp. 409–415, Apr. 1997.
[14] T. Kageyama *et al.*, "High efficiency 1060 nm VCSELS for low power consumption," in *Proc. IEEE Int. Conf. Indium Phosphide Related Mater.*, Newport Beach, CA, USA, 2009, pp. 391–396.
[15] T. Takeuchi, S. Kamiyama, M. Iwaya, and I. Akasaki, "GaN-based vertical-cavity surface-emitting lasers with AlInN/GaN distributed bragg reflectors," *Rep. Prog. Phys.*, vol. 82, no. 1, Nov. 2018, Art. no. 012502.
[16] E. Hashemi *et al.*, "Engineering the lateral optical guiding in gallium nitride-based vertical-cavity surface-emitting laser cavities to reach the lowest threshold gain," *Japanese J. Appl. Phys.*, vol. 52, no. 8, Aug. 2013, Art. no. 08JG04.
[17] J. T. Leonard *et al.*, "Nonpolar III-nitride vertical-cavity surface-emitting lasers incorporating an ion implanted aperture," *Appl. Phys. Lett.*, vol. 107, no. 1, Jul. 2015, Art. no. 011102.
[18] J. T. Leonard *et al.*, "Nonpolar III-nitride vertical-cavity surface-emitting laser with a photoelectrochemically etched air-gap aperture," *Appl. Phys. Lett.*, vol. 108, no. 3, Jan. 2016, Art. no. 031111.
[19] M. Kuramoto *et al.*, "Enhancement of slope efficiency and output power in GaN-based vertical-cavity surface-emitting lasers with a SiO_2-buried lateral index guide," *Appl. Phys. Lett.*, vol. 112, no. 11, Mar. 2018, Art. no. 111104.
[20] T. Hamaguchi *et al.*, "Lateral optical confinement of GaN-based VCSEL using an atomically smooth monolithic curved mirror," *Scientific Rep.*, vol. 8, Jul. 2018, Art. no. 10350.
[21] G. R. Hadley, "Effective index model for vertical-cavity surface-emitting lasers," *Opt. Lett.*, vol. 20, no. 13, Jul. 1995, Art. no. e16199.
[22] R. Michalzik, *Fundamentals, Technology and Applications of VerticalCavity Surface-Emitting Lasers*. Berlin, Germany: Springer, 2013.
[23] D. Ellafi *et al.*, "Effect of cavity lifetime variation on the static and dynamic properties of 1.3-μm wafer-fused VCSELs," *IEEE J. Sel. Topics Quantum*, vol. 21, no. 6, pp. 414–442, Mar. 2016.
[24] R. Butté *et al.*, "Room temperature polariton lasing in III-nitride microcavities: A comparison with blue GaN-based vertical cavity surface emitting lasers," in *Proc. Gallium Nitride Mater. Devices IV*, San Jose, CA, USA, 2009, Art. no. 721619-7.
[25] E. Hashemi *et al.*, "Analysis of structurally sensitive loss in GaN-based VCSEL cavities and its effect on modal discrimination," *Opt. Express*, vol. 22, no. 1, pp. 411–426, Jan. 2014.
[26] Y. Mei *et al.*, "A comparative study of thermal characteristics of GaN-based VCSELs with three different typical structures," *Semicond. Sci. Technol.*, vol. 33, Dec. 2017, Art. no. 015016.
[27] A. Sharma, J. M. Yarrison-Rice, H. E. Jackson, and K. D. Choquette, "Near-field spectroscopic characterization of a 10 μm aperture selectively oxidized vertical cavity surface emitting laser," *J. Appl. Phys.*, vol. 92, no. 11, pp. 6837–6844, Aug. 2002.
[28] S. P. Hegarty, G. Huyet, J. G. McInerney, K. D. Choquette, K. M. Geib, and H. Q. Hou, "Size dependence of transverse mode structure in oxide-confined vertical-cavity laser diodes," *Appl. Phys. Lett.*, vol. 73, no. 24, pp. 596–598, Aug. 1998.